Edelweiss Applied Science and Technology
ISSN: 2576-8484
Vol. 9, No. 4, 1332-1342
2025
Publisher: Learning Gate
DOI: 10.55214/25768484.v9i4.6261

Atomistic simulation of two-dimensional 1T-MnX2 sheets under uniaxial tension

Nguyen Huu Tu[1], Nguyen Van Thanh[1], Dang Van Manh[1], Nguyen Van Trang[2*]
[1]Faculty of Fundamental Science, Military Academy of Logistics, Hanoi, VietNam.
[2]Faculty of mechanical engineering, Thai Nguyen University of Technology, Vietnam; nvtrang@tnut.edu.vn (N.V.T.)

Abstract: We investigate the mechanical properties of two-dimensional 1T-MnX2 materials through the molecular dynamics finite element method with the Stillinger-Weber potential. The two-dimensional Young's modulus, Poisson's coefficient, maximum stress, and strain of these materials are examined for four 1T-MnX2 sheets. The effects of the armchair and zigzag directions on the mechanical properties under uniaxial tension are considered and discussed. Under uniaxial tension, we have determined the main mechanical properties. For 1T-MnO2, the maximum stress (σ t) was 16.794 N/m in the armchair direction, and the maximum elastic modulus (Et) was 154.96 N/m in the zigzag direction. For 1T-MnTe2, the maximum Poisson's ratio (ν) observed was 0.181 in the armchair direction. These materials are considered approximately isotropic and are characterized by brittle fracture. Simulation results will help to design and use two-dimensional 1T-MnX2 sheet-based nanocomposites and nanodevices.

Keywords: *IT structures, 2d-materials, Atomistic simulation, Stillinger-weber. Uniaxial tension.*

1. Introduction

This study focuses on determining the mechanical properties of two-dimensional materials that are compounds of transition metal Mn with non-metallic elements existing in the form of hexagonal structure 1T-MnX_2 Jiang and Zhou [1] where X is a non-metallic element. This polymorph can exist in nature or be created in the laboratory [1]. The structure of the 1T-MnX_2 material is shown in Figure. 1, through the orthogonal projection and the axial projection of a basic cell with the corresponding numbered atoms. Each basic cell (the rectangle drawn with dashed lines in Figure. 1) with side size a (Å) contains 9 atoms including 3 Mn atoms (red) on a plane, each Mn atom is bonded to 6 non-metallic atoms X (blue) distributed on two planes symmetrical to the plane containing Mn, the distance between the plane containing Mn and X is h; meanwhile, an X atom is bonded to 3 surrounding Mn atoms; X is one of the following elements: Oxygen (O), sulfur (S), selenium (Se), tellurium (Te). The material structure is more clearly shown through the material parameters including: the bond distance between two Mn and X atoms is d_{Mn-X}; the bond angle between X-Mn-X atoms is the angle θ_{MnXX}; Mn-X-Mn is the angle θ_{XMnMn} (see Table 1).

History: Received: 6 February 2025; Revised: 4 April 2025; Accepted: 8 April 2025; Published: 15 April 2025
* Correspondence: nvtrang@tnut.edu.vn

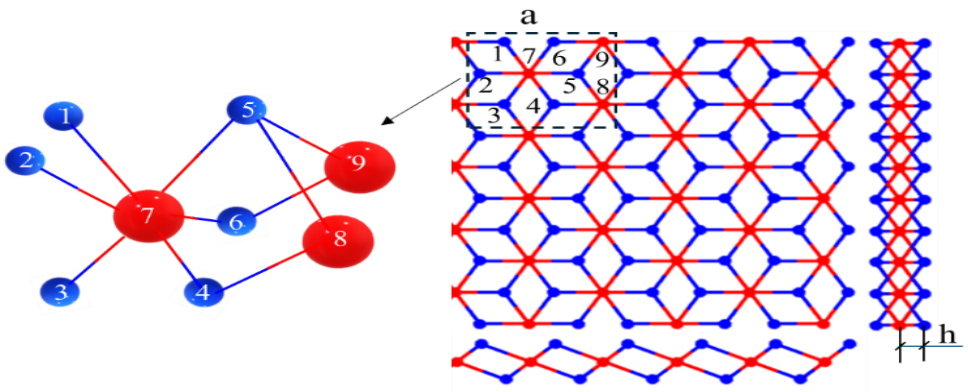

Figure 1.
Schematic illustration of: 1T-MnX_2 structures (X= O, S, Se and Te are non-metallic elements).

Table 1.
Material network parameters of 1T-MnX_2 materials.

No.	Materials	Lattice constant, a (Å)	$d_{Mn\text{-}X}$(Å)	θ_{MnXX}(°)	θ_{XMnMn}(°)
1	1T-MnO_2	2.82	1.88	97.181	97.181
2	1T-MnS_2	3.12	2.27	86.822	86.822
3	1T-$MnSe_2$	3.27	2.39	86.330	86.330
4	1T-$MnTe_2$	3.54	2.59	86.219	86.219

Source: Jiang and Zhou [1].

Various the two-dimensional (2D) materials are existed in many different structural forms such as Pucked structure Lê Minh, et al. [2] planar hexagonal graphene Geim [3], low-bucked silicene, BN and AlN [4], 1H and 1T structures [1]. These materials exhibit exceptional properties, including high electrical and thermal conductivity, and remarkable mechanical strength. They exhibit good mechanical properties with high elastic modulus of ~0.5-1 TPa and tensile strength of ~61 GPa [5]. They possess distinguishable chemical and thermal stability with high oxidation resistance up to 900^0 C in air [6], wide band-gaps independent of tube structures [7, 8]. Excellent thermal conductivity [9]. They are also an effective violet and ultra-violet light emission material [10, 11]. Interestingly, their mechanical behavior at the nanoscale can differ significantly from macroscopic observations, showcasing phenomena like a negative Poisson's ratio [2, 12]. And extreme hardness (e.g., graphene being harder than diamond) [13]. Furthermore, their bandgap can be tailored through the application of mechanical strain [14-16] or external electric fields, without requiring any chemical alterations [16-18]. Their versatility has led to their incorporation into electronic devices for manufacturing nanometer-sized transistors [1, 3, 16]. electronic storage devices [19, 20]. And applications within the energy [21, 22]. And medical fields [23, 24]. Such applications require a deep comprehension of the mechanical properties and performance of 1T-MnX_2 materials under various loading conditions. Characterizing the mechanical properties of nanoscale materials presents significant experimental challenges due to difficulties in manipulation, high costs, and often infeasibility. Consequently, researchers often rely on computational methods like experimental simulation (e.g., atomic finite element method (AFEM) [25-27]. Molecular dynamics (MD) [28]. First-principles [29, 30]. And ab initio calculations [31] to predict these properties.

The Mechanical properties of 1T-MnX_2 materials seem still unexplored by MDFEM method. It should be noted that the Mechanical properties of these materials has been investigated by molecular dynamics (MD) method see e. g. Jiang and Zhou [1] and references therein. The present work investigates through molecular dynamics finite element method (MDFEM) the mechanical properties of two-dimensional 1T-MnX_2 materials under uniaxial tension. The effects of the armchair and zigzag directions to the mechanical properties of these materials under uniaxial tension are studied and discussed.

Edelweiss Applied Science and Technology
ISSN: 2576-8484
Vol. 9, No. 4: 1332-1342, 2025
DOI: 10.55214/25768484.v9i4.6261

2. Framework for Analysis

While density functional theory (DFT) calculations and molecular dynamics (MD) simulations are time-consuming, molecular dynamic finite element methods (MDFEM), sometime known as atomic-scale finite element methods or atomistic finite element methods, have been developed to analyze nanostructured materials in a computationally efficient way, see e. g. [25, 28]. To achieve the atomic positions of the BN-NT under specific boundary conditions, molecular dynamic finite element method (MDFEM) is here adopted. In MDFEM, atoms and atomic displacements are considered as nodes and translational degrees of freedom (nodal displacements), respectively. Both first and second derivatives of system energy are used in the energy minimization computation, hence it is faster than the standard conjugate gradient method which uses only the first order derivative of system energy as discussed in [32]. The stiffness matrices of these elements are established based upon interatomic potentials. Similar to conventional finite element method, global stiffness matrix is assembled from element stiffness matrices. Hence, relations between atomic displacement and force can be derived by solving a system of equations.

For each 1T-MnX_2 sheet, the atomic interaction potential is determined through the parameters of the Stillinger-Weber potential function including the direct binding energy of two adjacent atoms (Er, eV) and the binding energy of three adjacent atoms (E_θ, eV) through the following equations:

$$E = E_r + E_\theta \tag{1}$$

$$E_r = \sum_{i=1}^{m} V_2 \tag{2}$$

$$E_\theta = \sum_{i=1}^{n} V_3 \tag{3}$$

$$V_2 = Ae^{\left[\rho/\left(r_{ij}-r_{max}\right)\right]}\left(B/r_{ij}^4-1\right) \tag{4}$$

$$V_3 = Ke^{\left[\rho_{ij}/\left(r_{ij}-r_{max\,ij}\right)+\rho_{ik}/\left(r_{ik}-r_{max\,ik}\right)\right]}\left(\cos\left(\theta_{ijk}\right)-\cos\left(\theta_0\right)\right)^2 \tag{5}$$

In which, E is total atomic bond energy; E_θ(eV) is total angular bond energy of 3 atoms on the entire membrane; E_r(eV) is total linear bond energy between two atoms of the membrane; V_2(eV) is linear bond energy of two adjacent atoms; V_3(eV) is angular bond energy of 3 adjacent atoms; m and n are number of linear bonds and angular bonds in a calculation model; A(eV) and K(eV) are material coefficients; ρ(Å), B(Å^4), ρ_{ij}(Å), ρ_{ik}(Å), θ^o (degrees) are geometric parameters of the material; r_{ij}(Å), r_{ik}(Å) are bond length between two atoms i, j and k respectively; θ_{ijk} (degrees) is bond angle between three atoms i, j, k (where i is the middle atom) (Figure. 2). These parameters are summarized in Tables 2 and 3.

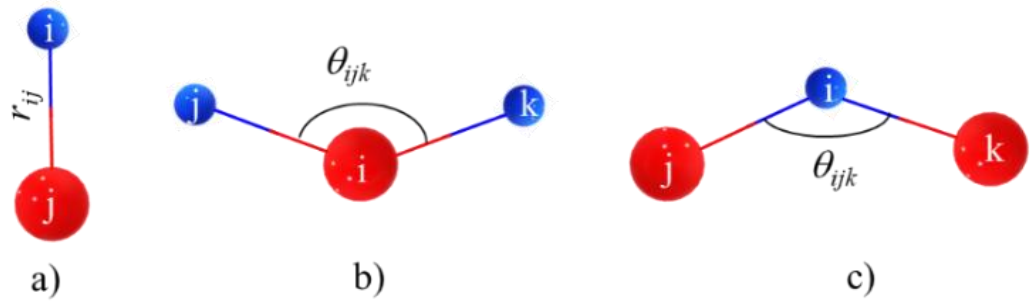

Figure 2.
Element model when using Stillinger-Weber potential function: a) Straight bond between two atoms; b,c) Angular bond between 3 atoms.

Edelweiss Applied Science and Technology
ISSN: 2576-8484
Vol. 9, No. 4: 1332-1342, 2025
DOI: 10.55214/25768484.v9i4.6261

Table 2.
Stillinger-Weber potential parameters for the straight bond of material 1T-MnX_2 [1].

No.	Materials	Bond	A, eV	ρ, Å	B, Å^4	r_{min}, Å	r_{max}, Å
1	1T-MnO_2	*Mn-O*	9.675	1.212	6.246	0.0	2.635
2	1T-MnS_2	*Mn-S*	3.127	1.111	13.276	0.0	3.064
3	1T-$MnSe_2$	*Mn-Se*	3.422	1.153	16.314	0.0	3.220
4	1T-$MnTe_2$	*Mn-Te*	4.007	1.246	22.499	0.0	3.488

Table 3.
Stillinger-weber potential parameters for angle bond of the 1T-MnX_2 [1].

No.	Materials	Angular bond	K, eV	θ_0, (°)	ρ_1, Å	ρ_2, Å	r_{min12}, Å	r_{max12}, Å	r_{min13} Å	r_{max13}, Å	r_{min23}, Å	r_{max23}, Å
1	1T-MnO_2	θ_{MnOO}	60.755	97.181	1.212	1.212	0.0	2.635	0.0	2.635	0.0	3.852
		θ_{OMnMn}	60.755	97.181	1.212	1.212	0.0	2.635	0.0	2.635	0.0	3.852
2	1T-MnS_2	θ_{MnSS}	19.765	86.822	1.111	1.111	0.0	3.064	0.0	3.064	0.0	4.262
		θ_{SMnMn}	19.765	86.822	1.111	1.111	0.0	3.064	0.0	3.064	0.0	4.262
3	1T-$MnSe_2$	θ_{MnSeSe}	19.390	86.330	1.153	1.153	0.0	3.220	0.0	3.220	0.0	4.467
		θ_{SeMnMn}	19.390	86.330	1.153	1.153	0.0	3.220	0.0	3.220	0.0	4.467
4	1T-$MnTe_2$	θ_{MnTeTe}	19.307	86.219	1.246	1.246	0.0	3.488	0.0	3.488	0.0	4.836
		θ_{TeMnMn}	19.307	86.219	1.246	1.246	0.0	3.488	0.0	3.488	0.0	4.836

For each 1T-MnX_2 membrane, the total number of atoms is N; $\mathbf{X}_i$ and $\boldsymbol{u}_i$ are the initial coordinates and displacement of the i-th atom; then, the coordinates of the atom after deformation are $\mathbf{x}_i=\mathbf{X}_i+\boldsymbol{u}_i$. The atomic interaction potential of the entire membrane calculated by formula (1) is an equation that depends on the coordinates of each atom on the membrane as follows:

$$E = E\left(\boldsymbol{x}_1, \boldsymbol{x}_2, ..., \boldsymbol{x}_N\right) \tag{6}$$

On the other hand, when the membrane is subjected to an external force f_i on the i-th atom (considered as nodes), the atoms in the membrane have displacements ui correspondingly, the potential energy of the applied external force is calculated as follows

$$E_{ext} = \sum_{i=1}^{N} \boldsymbol{f}_i \boldsymbol{u}_i \tag{7}$$

The total potential energy of the membrane is

$$\Pi = E - E_{ext} \tag{8}$$

The membrane is in equilibrium when the total potential energy reaches its minimum value according to the principle of minimum potential energy. Therefore, the first derivative of the total potential energy will be zero as shown in Eq. (9)

$$\frac{\partial \Pi}{\partial \boldsymbol{u}_i} = 0; \; i = 1 \div N \tag{9}$$

Solving the system of equations (9), the displacement of all atoms in the membrane is determined. In the experimental simulation using the atomic finite element method, solving the system of equations (9) using the Newton–Raphson iteration method, the use of this method has been clearly shown in [25, 27, 28], then the equation in the form of finite elements is

$$\boldsymbol{K}^{(k)}.\boldsymbol{u}^{(k)} = \boldsymbol{F}^{(k)} \tag{10}$$

Edelweiss Applied Science and Technology
ISSN: 2576-8484
Vol. 9, No. 4: 1332-1342, 2025
DOI: 10.55214/25768484.v9i4.6261

With

$$\boldsymbol{K}_{ij}^{k}=\frac{\partial^{2}\Pi^{(k)}}{\partial \boldsymbol{u}_{i}\partial \boldsymbol{u}_{j}};F_{i}^{(k)}=-\frac{\partial\Pi^{(k)}}{\partial \boldsymbol{u}_{i}}=f_{i}-\frac{\partial E^{(k)}}{\partial \boldsymbol{u}_{i}}; \tag{11}$$

Equations (10) and (11) are the basic equations of the finite element. With $\boldsymbol{K}^{(k)}$ being the global stiffness matrix, $\boldsymbol{u}^{(k)}$ being the nodal displacement vector and $\boldsymbol{F}^{(k)}$ being the nodal force vector. If each atom is considered as a node, the displacement of the atom is the displacement of the node. Due to the structure of the orthogonal hexagonal membrane, two types of elements are formed on the membrane, i.e., 3-node elements (Valence) are molecules on the boundary of the membrane, each element has 3 bonded atoms, 4-node elements (Improper) are elements inside the membrane, and each element is bonded by 4 atoms (Figure. 3). Since each atom can move in 3 directions, formula (11) is used to calculate the stiffness matrix of each element with dimensions $\left[\boldsymbol{K}_{Val}\right]_{9x9}^{(e)};\left[\boldsymbol{K}_{Imp}\right]_{12x12}^{(e)}$, corresponding to 3-node and 4-node elements. From the element stiffness matrix, calculate the global stiffness matrix $\left[\boldsymbol{K}\right]_{3Nx3N}^{(k)}$ which is the composite matrix of the element stiffness matrices over the entire membrane. The displacement vectors and force vectors have dimensions corresponding to the global stiffness matrix.

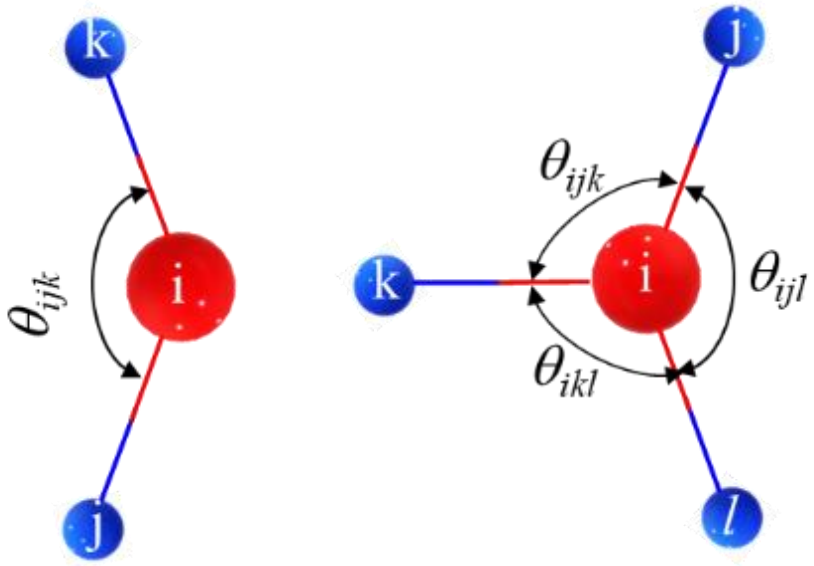

a) b)

Figure 3.
Element model using the atomic finite element method: a) the Valence element is formed by 3 adjacent atoms; b) the Improver element is formed by 4 adjacent atoms.

The system of equations (10) is solved by using the Newton–Raphson iteration method with displacement boundary conditions i.e., atoms on the tensile boundary have displacement equal to *u(0)*, and atoms on the retaining boundary (Figure. 4) have no displacement in the tensile direction. This is the experimental simulation method using molecular dynamic finite element method (MDFEM).

The The experimental model of the sheet tensile test is shown in Figure. 4 through the displacement method.

Edelweiss Applied Science and Technology
ISSN: 2576-8484
Vol. 9, No. 4: 1332-1342, 2025
DOI: 10.55214/25768484.v9i4.6261

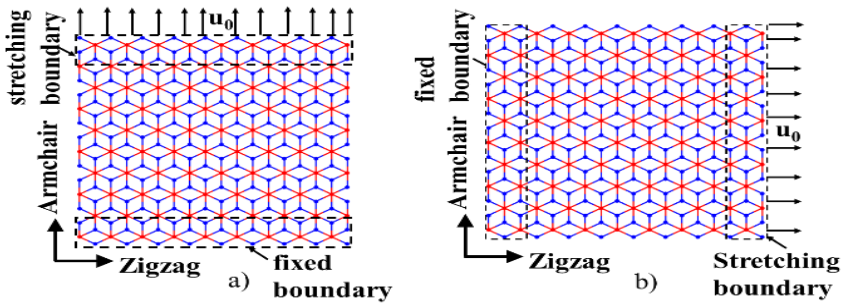

Figure 4.
The sheet with displacement boundary conditions under uniaxial tension: a) the armchair direction; b) the zigzag direction.

In the simulation, pull the rectangular sheet with approximately equal side dimensions (the rectangle is considered to be a square); each sheet has 4200 atoms; each stretching step causes the atoms on the stretching edge to move with an increment of δ_ε= 0.001, repeating until the sheet has a broken bond (the sheet is destroyed as shown in Figure. 6). At each step, equation (10) is solved to determine the displacement and nodal force of all atoms on the sheet at this step. The position of atoms in the next steps is determined as follows:

$$x_{(k+1)} = x_{(k)} + u_{(k)} \tag{12}$$

The iterative process continues until , with a given error, at which point the sheet is considered to have failed. The image of the failed sheet is shown in Figure. 6. The data of the entire experimental process, of all steps, is synthesized to determine the mechanical parameters that need to be calculated.

The tensile results of the 1T-MnX_2 materials are shown through the stress-strain relationship graph; the two-dimensional elastic modulus is determined by linearizing their relationship with strain in the range from 0 to 0.1; the Poisson's ratio is determined based on the ratio of transverse strain and axial strain; ν=-$\varepsilon_y/\varepsilon_x$; the two-dimensional tensile stress and tensile strain occur at the end of the tensile program. The stress-strain relationship when stretching the intact sheet of the four materials is shown in Figure. 5.

3. Results and Discussion

Figure 5 shows the stress-strain curves of the 1T-MnX_2 sheets in armchair and zigzag directions calculated by molecular dynamic finite element method (MDFEM). It can be seen from Figure 5 that the stress increases monotonously with an increase of the strain up to a maximum value and then drops suddenly. Therefore, the sheets exhibit a brittle fracture mechanism. Then, the maximum stress and strain at the maximum stress location replace the critical stress and critical strain, respectively.

Edelweiss Applied Science and Technology
ISSN: 2576-8484
Vol. 9, No. 4: 1332-1342, 2025
DOI: 10.55214/25768484.v9i4.6261

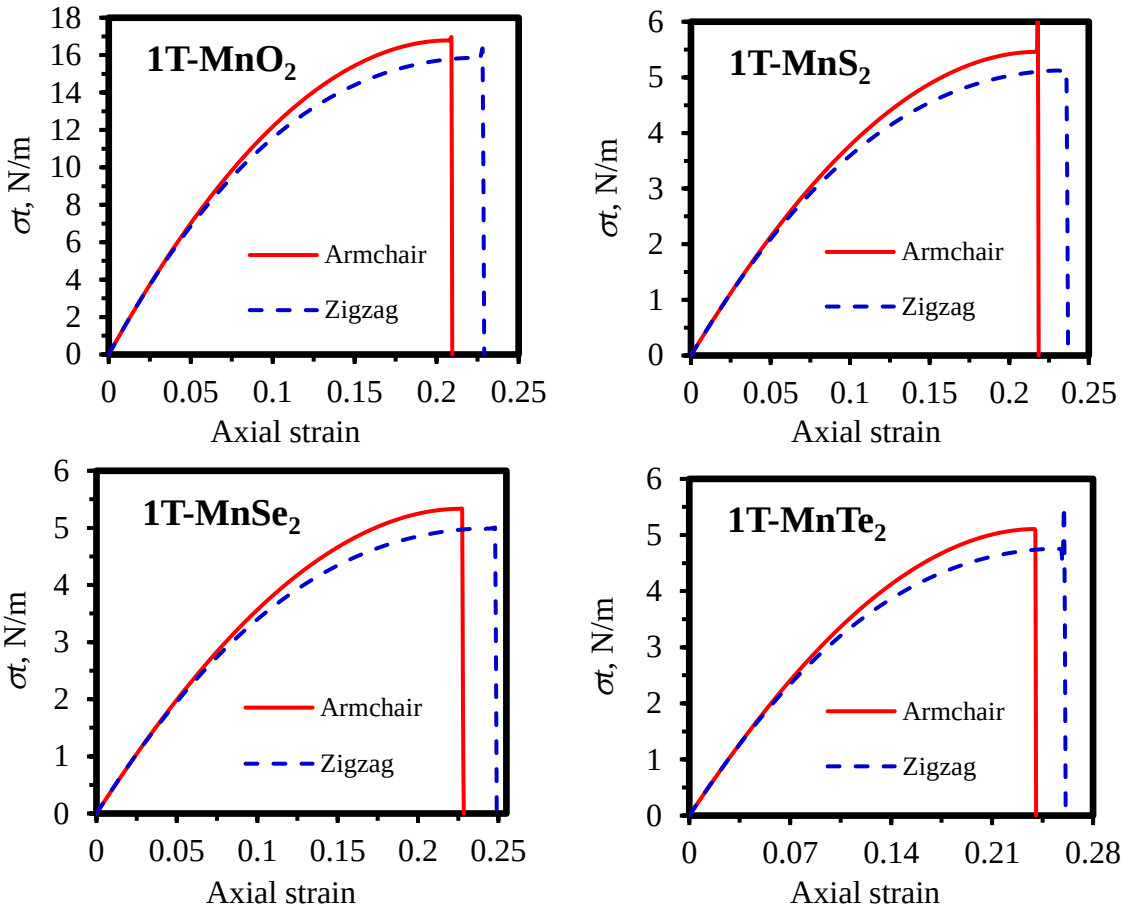

Figure 5.
The stress-strain curves of 1T-MnX_2 material sheets under uniaxial tension according to armchair and zigzag directions.

Table 4 shows the elastic modulus, maximum stress and maximum strain of 1T-MnX_2 material sheets according to armchair and zigzag directions calculated by MDFEM method. The results showed that maximum stress: σt=16.794N/m under uniaxial tension 1T-MnO2 in the armchair direction with strain ε=0.208; minimum stress: σt=4.752 N/m under uniaxial tension 1T-MnTe2 in the armchair direction with strain ε=0.256; maximum poisson's ratio: ν=0.181 under uniaxial tension 1T-MnTe2 in the armchair direction; minimum poisson's ratio: ν=0.121 under uniaxial tension 1T-MnO2 in the zigzag direction; maximum elastic modulus: Et=154.96 N/m under uniaxial tension 1T-MnO2 in the zigzag direction; minimum elastic modulus: Et=37.385 N/m under uniaxial tension 1T-MnTe2 in the armchair direction. These results showed that two-dimensional elastic modulus and poisson's ratio are approximately equal value when stretched in two directions armchair and zigzag. They are considered as approximately isotropic materials. In Table 4, these results were compared with the research results by Jiang under the same experimental simulation conditions but other method [1]. The comparison results showed that the errors were good agree.

Edelweiss Applied Science and Technology
ISSN: 2576-8484
Vol. 9, No. 4: 1332-1342, 2025
DOI: 10.55214/25768484.v9i4.6261

Table 4.
The mechanical parameters of four 1T-MnX_2 materials by MDFEM method.

No.	Materials	Directions	Elastic modulus *Et*, N/m	Poisson's ratio	Maximum stress σt, N/m	Tensile strain	Evaluations
1	1T-MnO_2	AC	153.900	0.123	16.794	0.208	Our results
			156.300	0.120	16.800	0.210	by MD at 1^0 K [1]
			-1.536	2.250	-0.035	-1.190	error (%) with [1]
		ZZ	154.960	0.121	15.883	0.224	Our results
			155.400	0.120	16.200	0.240	by MD at 1^0 K [1]
			-0.283	1.083	-1.957	-6.667	error (%) with [1]
2	1T-MnS_2	AC	46.159	0.147	5.468	0.218	Our results
			47.100	0.150	5.500	0.210	by MD at 1^0 K [1]
			-1.998	-1.800	-0.590	3.571	error (%) with [1]
		ZZ	46.500	0.145	5.143	0.235	Our results
			46.800	0.150	5.300	0.250	by MD at 1^0 K [1]
			-0.641	-3.400	-2.959	-6.000	error (%) with [1]
3	1T-$MnSe_2$	AC	42.726	0.162	5.338	0.227	Our results
			43.200	0.170	5.400	0.220	by MD at 1^0 K [1]
			-1.097	-4.765	-1.147	3.182	error (%) with [1]
		ZZ	43.083	0.160	4.996	0.246	Our results
			42.900	0.170	5.200	0.260	by MD at 1^0 K [1]
			0.427	-6.059	-3.916	-5.385	error (%) with [1]
4	1T-$MnTe_2$	AC	37.835	0.181	5.107	0.239	Our results
			38.500	0.190	5.200	0.240	by MD at 1^0 K [1]
			-1.727	-4.947	-1.792	-0.417	error (%) with [1]
		ZZ	38.206	0.178	4.752	0.256	Our results
			38.400	0.190	5.000	0.280	by MD at 1^0 K [1]
			-0.505	-6.105	-4.963	-8.571	error (%) with [1]

Figure 6 shows the destruction of the 1T-$MnSe_2$ sheet when stretching in the armchair direction with a strain of $\varepsilon = 0.227$; when stretching in the zigzag direction, at the step $\varepsilon = 0.246$, many bonds were broken and the sheet was destroyed.

.

Edelweiss Applied Science and Technology
ISSN: 2576-8484
Vol. 9, No. 4: 1332-1342, 2025
DOI: 10.55214/25768484.v9i4.6261

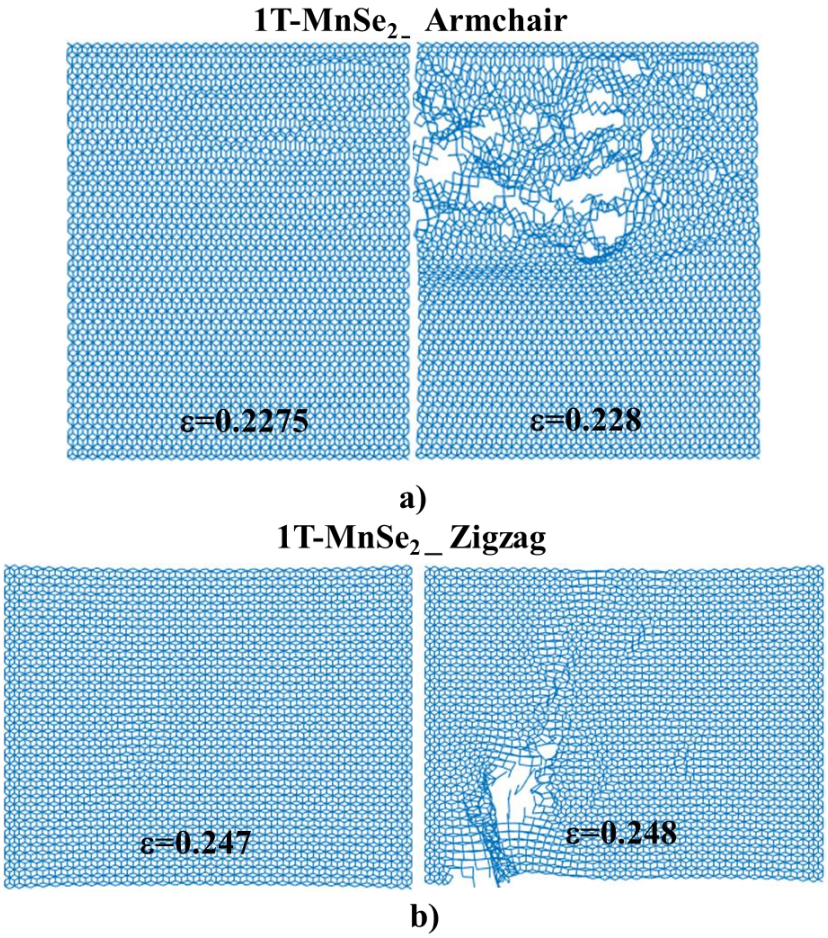

Figure 6.
Destroyed shapes of 1T-$MnSe_2$ sheets: a) uniaxial tension according to armchair; b) uniaxial tension according to zigzag.

4. Conclusions

We present the simulation results of the mechanical properties of 1T-MnX_2 nanosheets under uniaxial tension with the use of MDFEM with Stillinger-Weber potential. We have found maximum stress: σt=16.794N/m under uniaxial tension 1T-MnO_2 in the armchair direction with strain ε=0.208; minimum stress: σt=4.752 N/m under uniaxial tension 1T-$MnTe_2$ in the armchair direction with strain ε=0.256; maximum poisson's ratio: ν=0.181 under uniaxial tension 1T-$MnTe_2$ in the armchair direction; minimum poisson's ratio: ν=0.121 under uniaxial tension 1T-MnO_2 in the zigzag direction; maximum elastic modulus: Et=154.96 N/m under uniaxial tension 1T-MnO_2 in the zigzag direction; minimum elastic modulus: Et=37.385 N/m under uniaxial tension 1T-$MnTe_2$ in the armchair direction. These materials generally behave as approximately isotropic substances and exhibit brittle fracture characteristics. These results will help to design and use two-dimensional 1T-MnX_2 sheets based nanocomposites and nanodevices.

Edelweiss Applied Science and Technology
ISSN: 2576-8484
Vol. 9, No. 4: 1332-1342, 2025
DOI: 10.55214/25768484.v9i4.6261

Transparency:

The authors confirm that the manuscript is an honest, accurate, and transparent account of the study; that no vital features of the study have been omitted; and that any discrepancies from the study as planned have been explained. This study followed all ethical practices during writing.

Authors' Contributions:

The idea of the paper was proposed by Nguyen Van Trang and Nguyen Huu Tu. The simulation and the calculation were conducted by Nguyen Van Thanh and Dang Van Manh. The manuscript was written by Nguyen Van Trang with support from Nguyen Huu Tu. All authors have read and agreed to the manuscript.

Acknowledgements:

This word has been supported by the Thai Nguyen University of Technology, Thai Nguyen University.

References

[1] J.-W. Jiang and Y.-P. Zhou, "Parameterization of Stillinger-Weber potential for two-dimensional atomic crystals," *arXiv preprint arXiv:1704.03147*, 2017. https://doi.org/10.48550/arXiv.1704.03147

[2] Q. Lê Minh, T. N. Hữu, L. Đ. T. Kim, and T. N. Văn, "Mô phỏng kéo màng vật liệu hai chiều đa nguyên tử cấu trúc nếp gấp," *Tạp chí Khoa học Giao thông vận tải*, vol. 73, no. 5, pp. 514-526, 2022.

[3] A. K. Geim, "Graphene: status and prospects," *science*, vol. 324, no. 5934, pp. 1530-1534, 2009.

[4] H.-T. Nguyen, M.-Q. Le, and V.-T. Nguyen, "Mode-I stress intensity factors of silicene, AlN, and SiC hexagonal sheets," *Materials Research Express*, vol. 5, no. 6, p. 065025, 2018.

[5] R. Arenal, M.-S. Wang, Z. Xu, A. Loiseau, and D. Golberg, "Young modulus, mechanical and electrical properties of isolated individual and bundled single-walled boron nitride nanotubes," *Nanotechnology*, vol. 22, no. 26, p. 265704, 2011. https://doi.org/10.1088/0957-4484/22/26/265704

[6] Y. Chen, J. Zou, S. J. Campbell, and G. Le Caer, "Boron nitride nanotubes: pronounced resistance to oxidation," *Applied physics letters*, vol. 84, no. 13, pp. 2430-2432, 2004. https://doi.org/10.1063/1.1667278

[7] B. Baumeier, P. Krüger, and J. Pollmann, "Structural, elastic, and electronic properties of SiC, BN, and BeO nanotubes," *Physical Review B*, vol. 76, no. 8, p. 085407, 2007. https://doi.org/10.1103/PhysRevB.76.085407

[8] G. Guo, S. Ishibashi, T. Tamura, and K. Terakura, "Static dielectric response and Born effective charge of BN nanotubes from ab initio finite electric field calculations," *Physical Review B*, vol. 75, no. 24, p. 245403, 2007.

[9] C. Chang *et al.*, "Isotope effect on the thermal conductivity of boron nitride nanotubes," *Physical review letters*, vol. 97, no. 8, p. 085901, 2006.

[10] C. Attaccalite, L. Wirtz, A. Marini, and A. Rubio, "Efficient Gate-tunable light-emitting device made of defective boron nitride nanotubes: from ultraviolet to the visible," *Scientific reports*, vol. 3, 2013.

[11] L. H. Li, Y. Chen, M.-Y. Lin, A. M. Glushenkov, B.-M. Cheng, and J. Yu, "Single deep ultraviolet light emission from boron nitride nanotube film," *Applied physics letters*, vol. 97, no. 14, p. 141104, 2010.

[12] L. Yu, Q. Yan, and A. Ruzsinszky, "Negative Poisson's ratio in 1T-type crystalline two-dimensional transition metal dichalcogenides," *Nature communications*, vol. 8, no. 1, pp. 1-8, 2017.

[13] M.-Q. Le and R. C. Batra, "Mode-I stress intensity factor in single layer graphene sheets," *Computational Materials Science*, vol. 118, pp. 251-258, 2016.

[14] D. Singh, S. K. Gupta, I. Lukačević, and Y. Sonvane, "Indiene 2D monolayer: a new nanoelectronic material," *RSC advances*, vol. 6, no. 10, pp. 8006-8014, 2016.

[15] Z. Zhu and D. Tománek, "Semiconducting layered blue phosphorus: a computational study," *Physical review letters*, vol. 112, no. 17, p. 176802, 2014.

[16] J.-A. Yan, S.-P. Gao, R. Stein, and G. Coard, "Tuning the electronic structure of silicene and germanene by biaxial strain and electric field," *Physical Review B*, vol. 91, no. 24, p. 245403, 2015. https://doi.org/10.1103/PhysRevB.91.245403

[17] A. Molle, J. Goldberger, M. Houssa, Y. Xu, S.-C. Zhang, and D. Akinwande, "Buckled two-dimensional Xene sheets," *Nature materials*, vol. 16, no. 2, pp. 163-169, 2017.

[18] Z. Ni *et al.*, "Tunable bandgap in silicene and germanene," *Nano letters*, vol. 12, no. 1, pp. 113-118, 2012.

[19] F. H. Stillinger and T. A. Weber, "Computer simulation of local order in condensed phases of silicon," *Physical review B*, vol. 31, no. 8, p. 5262, 1985.
[20] J. Tersoff, "Modeling solid-state chemistry: Interatomic potentials for multicomponent systems," *Physical review B*, vol. 39, no. 8, p. 5566, 1989. https://doi.org/10.1103/PhysRevB.39.5566
[21] P. Vishnoi, K. Pramoda, and C. Rao, "2D elemental nanomaterials beyond graphene," *ChemNanoMat*, vol. 5, no. 9, pp. 1062-1091, 2019.
[22] D. Geng and H. Y. Yang, "Recent advances in growth of novel 2D materials: beyond graphene and transition metal dichalcogenides," *Advanced Materials*, vol. 30, no. 45, p. 1800865, 2018. https://doi.org/10.1002/adma.201800865
[23] F. Wang *et al.*, "2D library beyond graphene and transition metal dichalcogenides: a focus on photodetection," *Chemical Society Reviews*, vol. 47, no. 16, pp. 6296-6341, 2018.
[24] B. Liu and K. Zhou, "Recent progress on graphene-analogous 2D nanomaterials: Properties, modeling and applications," *Progress in Materials Science*, vol. 100, pp. 99-169, 2019.
[25] B. Liu, Y. Huang, H. Jiang, S. Qu, and K. Hwang, "The atomic-scale finite element method," *Computer methods in applied mechanics and engineering*, vol. 193, no. 17-20, pp. 1849-1864, 2004.
[26] D.-T. Nguyen, M.-Q. Le, T.-L. Bui, and H.-L. Bui, "Atomistic simulation of free transverse vibration of graphene, hexagonal SiC, and BN nanosheets," *Acta Mechanica Sinica*, vol. 33, pp. 132-147, 2017.
[27] Y. Wang *et al.*, "Atomistic finite elements applicable to solid polymers," *Computational materials science*, vol. 36, no. 3, pp. 292-302, 2006.
[28] J. Wackerfuß, "Molecular mechanics in the context of the finite element method," *International Journal for Numerical Methods in Engineering*, vol. 77, no. 7, pp. 969-997, 2009. https://doi.org/10.1002/nme.2442
[29] B. Mortazavi, O. Rahaman, M. Makaremi, A. Dianat, G. Cuniberti, and T. Rabczuk, "First-principles investigation of mechanical properties of silicene, germanene and stanene," *Physica E: Low-dimensional Systems and Nanostructures*, vol. 87, pp. 228-232, 2017. https://doi.org/10.1016/j.physe.2016.10.047
[30] F. Hao and X. Chen, "First-principles study of the defected phosphorene under tensile strain," *Journal of Applied Physics*, vol. 120, no. 16, 2016.
[31] J. Pokluda, M. Černý, M. Šob, and Y. Umeno, "Ab initio calculations of mechanical properties: Methods and applications," *Progress in Materials Science*, vol. 73, pp. 127-158, 2015. https://doi.org/10.1016/j.pmatsci.2015.04.001
[32] B. Liu, Y. Huang, H. Jiang, S. Qu, and K. C. Hwang, "The atomic-scale finite element method," *Computer Methods in Applied Mechanics and Engineering*, vol. 193, pp. 1849-1864, 2004.

Edelweiss Applied Science and Technology
ISSN: 2576-8484
Vol. 9, No. 4: 1332-1342, 2025
DOI: 10.55214/25768484.v9i4.6261